

Tantalum electrodeposition on glass-ceramic substrate - compositional and structural analyses

Helena Simunkova^{a,b*}, Eva Kolibalova^b, Lukas Kalina^c, Adam Whitehead^d, Ondrej Caha^{b,e}, Zdenek Spotz^b, Tomáš Lednický^{b,f}, Jaromir Hubalek^{a,b}

^a Department of Microelectronics, Brno University of Technology (BUT), Technicka 3058/10, Kralovo Pole, 61600 Brno, Czech Republic

^b Central European Institute of Technology (CEITEC), BUT, Purkynova 123, 621 00 Brno-Medlanky, Czech Republic

^c Faculty of Chemistry, Brno University of Technology (BUT), Purkynova 464/118, Brno 612 00, Czech Republic

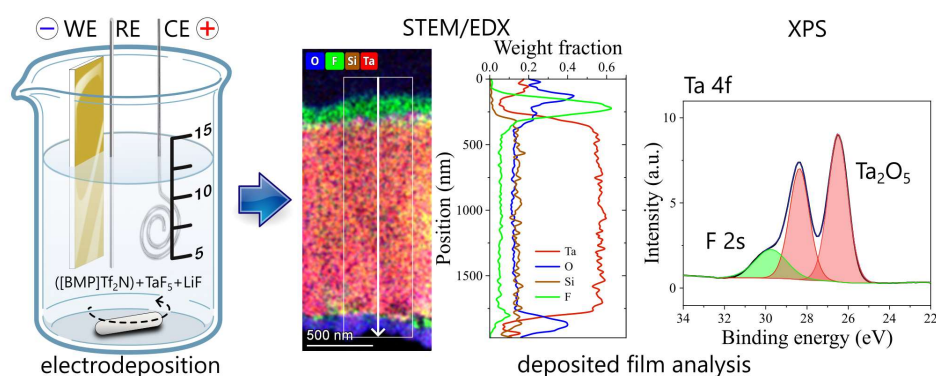
^d Invinity Energy (UK) Ltd., United Kingdom

^e Department of condensed matter physics, Masaryk University, Kotlarska 2, 61137 Brno, Czech Republic

^f Leibniz Institute of Photonic Technology, Albert-Einstein-Str. 9, 07745 Jena, Germany

*Corresponding author: simunkova@vutbr.cz

Abstract. Electrodeposition of tantalum thin coating was attempted from a room temperature ionic liquid, BMP[Tf_2N] in presence of dissolved TaF_5 and LiF . The influence of deposition parameters, such as ionic liquid composition, substrate type, electrical potential or temperature upon structure and composition was observed. Cyclic voltammetry, scanning transmission electron microscopy (STEM) in conjunction with energy dispersive X-ray analysis (EDX), X-ray photoelectron spectroscopy (XPS), as well as X-ray diffraction (XRD) techniques were applied. The reversibility of the reduction processes was examined, and comparison made to deposition from molten salt systems.



Keywords: Tantalum electrodeposition; ionic liquid; oxyfluorides; scanning transmission electron microscopy; energy dispersive X-ray analysis, irreversible electroreduction

1. Introduction

Tantalum (Ta) is a common refractory metal, which is hard, ductile and a good heat conductor [1]. It is also known for its excellent resistance against acidic corrosion, which is due in part to the presence of tantalum pentoxide (Ta_2O_5) passivation layer. Ta_2O_5 is promising sensing material with very stable humidity and hydrogen sensitivity [2, 3] and detection of ammonia was recently presented [4]. Moreover, Ta is biocompatible and is thus used as surface treatment for biomedical implants [1, 5, 6, 7]. Unfortunately, it cannot be electrodeposited from aqueous solutions. Electrodeposition from ionic liquids might be an alternative to the traditional deposition techniques (PVD, CVD and molten salts depositions). Some authors have already studied Ta electrodeposition from ionic liquids in detail [8, 9]. They achieved a thin crystalline Ta layer (up to 1 μm), deposited on certain substrates (such as platinum) [10]. Nahra *et al.* [1] studied the influence of working electrode material on the adherence and thickness of Ta electrodeposits. Gold deposited on quartz single crystal, borosilicate glass or mica substrates [10, 11, 12] were often applied as the working electrode materials. It was found that the mechanical quality and the adherence of the electrodeposits improved as the temperature increased (up to 200°C), as well as upon addition of lithium fluoride to the electrolyte [10, 12]. The reduction of Ta was proven to be a complex process. Both, reversible [13, 14] and irreversible [1, 15] Ta redox reactions were determined and described in the literature. It has been repeatedly stated that electrodeposition of tantalum at elevated potentials lead to irreversibility. Nahra *et al.* observed irreversible behavior in the case of ionic liquids [1], whereas Polyakova *et al.* [15] published similar phenomenon in the molten salt system, FLINAK. Polyakova *et al.* [15] determined three separate reduction steps in FLINAK. By means of titration with sodium monoxide and coincident voltammetry, the influence of oxide concentration upon the redox reactions was observed [15]. The first reduction process was assigned to TaF_7^{2-} reduction to tantalum metal in a single five-electron step. The second

voltammetry peak was attributed to reduction of the oxyfluoride, $TaOF_5^{2-}$ ions to tantalum metal, also by a single five-electron step and the last step was elucidated as $TaO_2F_x^{(x-1)-}$ reduction [15]. The last two reactions of the mono and di-oxyfluorides were analyzed as irreversible, whereas the first reduction of the tantalum fluorides was quasi-reversible [15]. The changes in the reversibility were caused by the oxide concentration variation. It was noted elsewhere that oxides are very reactive towards tantalum fluorides leading to a formation of tantalum oxyfluorides: $TaOF_5^{2-}$ and $TaO_2F_x^{(x-1)-}$ [16]. Similar studies were performed by Lantelme *et al.* [13] and by Chamelot *et al.* [14], where the single step tantalum reduction was shown, as well as the formation of tantalum oxyfluorides and their reduction at more negative potentials. Contrary to Polyakova, the reduction of TaF_7^{2-} to metallic tantalum was reversible in these two studies.

This work was undertaken to further understanding of tantalum electrodeposition from an ionic liquid.

2. Material and methods

Tantalum (Ta) electrodeposition was attempted using a room temperature ionic liquid (IL) 1-butyl-1-methylpyrrolidinium bis(trifluoro-methylsulfonyl) imide, ([BMP]Tf₂N) (Solvionic, 99.9 %), containing 0.25 M – 0.5 M of both TaF₅ (Alfa Aesar, 99.9 %) and LiF (Alfa Aesar, 99.99 %). The salts were dissolved in the IL and held for about 1 hour at 120°C to remove trace H₂O. Ta was electrodeposited potentiostatically at -1.5 or -1.7 V vs. a platinum wire pseudo reference electrode, in a glove box under inert gas N₂ (H₂O, O₂ < 15 ppm), at 150 °C and 200 °C. An Autolab PGSTAT204/FRA32M (Metrohm) was used as the current source. The same glass flask, covered with a PTFE lid, holding the working and reference electrodes, was used for both deposition and voltammetry. The counter electrode was a Pt wire. The working electrode was a planar glass-ceramic Sitall substrate, covered with polycrystalline gold (Au) (ca. 300 nm thick, on a 20 nm thick

Ni/Cr layer, made by PVD) or niobium (Nb) (ca. 560 nm thick). The **cyclic voltammetry** of 0.25 M (TaF₅ and LiF) ionic liquid solution upon Au deposited SiTall was performed from the open circuit potential of about -0.3 V vs. Pt, starting by scanning cathodically. Several potential ranges were employed, up to +/- 3.5 V vs. Pt. The scan rate was either 5 or 10 mVs⁻¹, at temperatures of 25°C or 200°C.

Transmission electron microscopy (**TEM**) and scanning transmission electron microscopy (**STEM**) using Thermo Fisher Scientific Titan Themis 60-300 (scanning) transmission electron microscope operated at 300 kV was utilized to investigate the coating cross-section prepared in Focused ion beam (**FIB**) / scanning electron microscope FEI Helios NanoLab 660. Energy-dispersive x-ray spectroscopy (**EDX**) was used to determine the atomic composition of the coated layers. The EDX analyses were conducted at the acceleration voltage of 300 kV. Two Ta specimens were tested: the first one was prepared by cyclic voltammetry (no stirring) from -1.4 V to -1.7 V vs. Pt and back to -1.4 V at 200°C, the second one was deposited at a constant potential of -1.7 V vs. Pt at 150°C and 900 rpm stirring rate. The TaF₅ and LiF was 0.4 M and 0.25 M, respectively. Thermal post-treatment at 800°C for 6 h and pressure ranging from 10⁻³ to 10⁻⁴ Pa was carried out of the second specimen.

X-ray photoelectron spectroscopy (**XPS**) analyses were carried out with an Axis Ultra DLD spectrometer using a monochromatic Al K α (h ν = 1486.7 eV) X-ray source operating at 150 W (10 mA, 15 kV). The spectra were obtained using an analysis area of ~300 × 700 μ m². The Kratos charge neutralizer system was used for all analyses. High-resolution spectra were measured with a step size of 0.1 eV and 20 eV pass energy. The instrument base pressure was 2 · 10⁻⁸ Pa. Spectra were analyzed using CasaXPS software (version 2.3.15) and have been charge corrected to the main line of the carbon C 1s spectral component (C–C, C–H) set to 284.80 eV. A standard Shirley background was used for all sample spectra. The deposition was made at 150 °C and 2 ionic liquid

stirring rates – 500 or 900 rpm. The working electrode potential was either -1.5 or -1.7 V vs. Pt. The analysis was performed of Ta deposits upon Sitall with either Nb or Au metal coating as a conductive intermediate. An influence of the intermediate metal coating was excluded by several XPS studies. Comparable plating parameters resulted in comparable XPS spectra regardless Au or Nb intermediate.

The X-ray diffraction (**XRD**) measurement was performed using small, collimated beam and 2D detector to obtain signal from small sample area. The measured data were averaged along Debye ring in the angular range of 15 degrees. The analysis was performed on annealed Ta-based coating electrodeposited on Nb coated Sitall substrate from 0.25 M solution at 150 °C and 900 rpm stirring rate (same as the second STEM specimen).

3. Results and discussion

3.1. Cyclic voltammetry

The tantalum electrodeposition was combined with cyclic voltammetry experiments. The voltammetry at 25 °C for the ([BMP]Tf₂N) ionic liquid containing 0.25 M TaF₅ and 0.25 M LiF on polycrystalline gold electrode was performed, see Fig. 1 (a). The anodic sweep followed the cathodic one. At 200 °C, the current density was ten times higher than at 25 °C, see Fig. 1 (b) and (c). In our study, we determined both reversible, as well as irreversible redox processes, in line with the literature (as described above). Trials at room temperature, 120 °C and 150 °C were performed, but a visible, thick black coating was only obtained at 150 °C and 200 °C and none at room temperature. It has been published elsewhere that the adhesion and crack formation improve with elevated temperature [12, 17, 18]. According to our previous findings, the anodic steps beyond +1 V vs. Pt might be attributed to disintegration of the Au/NiCr underlayers and to an irreversible Tf₂N⁻ anion oxidation starting at about +2.4 V vs. Pt. The electrochemical window

of the ([BMP]Tf₂N) ionic liquid was estimated elsewhere to be about 5.75 V going from -3.4 V (vs. Pt-Fc/Fc⁺) to +2.35V (vs. Pt-Fc/Fc⁺) (det. on platinum working electrode at 40 °C and 50 mV s⁻¹ scan rate) [11].

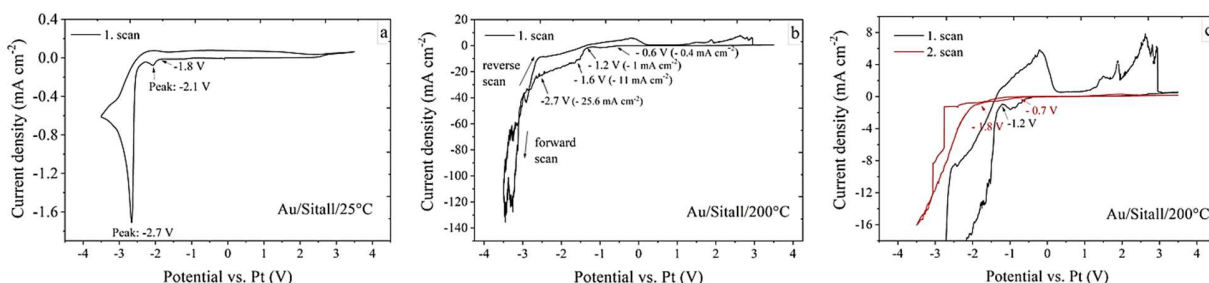


Fig. 1. Cyclic voltammogram of ([BMP]Tf₂N) containing 0.25 M TaF₅ and 0.25 M LiF on gold at (a) 25 °C, (b) 200 °C, (c) 200 °C (2 scans in sequence). Scan rate was 10 mV s⁻¹ in all cases.

Moreover, the overall redox reactions at a short switching potential range (-1.6 to +0.5 V) revealed quasi-reversible behavior, see Fig. 2. The anodic peak area was about 37 – 48 % of the cathodic one, determined at 2 – 10 mV s⁻¹, respectively. The anodic/cathodic reaction ratio increased with the scan rate at the range 2 - 10 mV s⁻¹. The calculation was done for all cathodic and anodic peaks related to the Ta-based redox reactions. The low anodic/cathodic ratio indicates that the redox processes were only quasi-reversible. Irreversible behavior was observed at a potential range of +/- 3.5 V, see Fig. 1. Especially at the second cyclic step, a quasi-reversible redox reaction turned into completely irreversible one, performed on the same piece of a working electrode, see Fig. 1 (c). The first scan in the cathodic direction resulted in currents about 10 times higher than in the second scan. Moreover, the reduction start potential was about 600 mV more negative in the second scan compared to the first one. The anodic reverse oxidation disappeared completely in the second scan accounting for irreversible behavior. We suppose that the change in reversibility resulted from the choice of the working electrode material, glass-ceramic, which was attacked by fluoride ions and released oxide ions in turn. These oxide ions were able to complex the tantalum

ions giving tantalum oxyfluorides, which might be reduced to some oxidized tantalum compound. The black appearance of most of our deposits indicated a presence of insoluble, oxidized compound(s) on top of the coatings. Black colored coatings were determined previously too [13]. At the large potential limit (± 3.5 V) experiment, as shown in Fig. 1, the ionic liquid solution even became black in color due to a powdery black deposit being released into the solution. Similarly, Nahra *et al.* [11] observed that at potentials higher than -2.4 V (vs. Pt-Fc/Fc⁺) a black powder stripped from the working electrode surface to the electrolyte. It was determined elsewhere that Ta electroreduction from molten salt systems proceed as a single five-electron reduction step [13, 14, 15]. A single step reduction involving n electrons is considered as a multistep reaction, where n is the number of single electron transfer steps which can be rapid and remain undetected at the usual time scales [13].

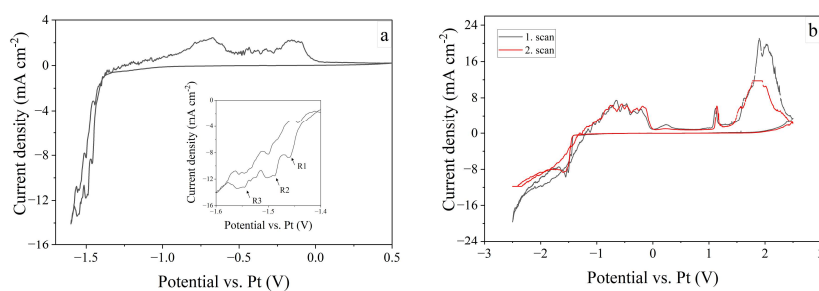


Fig. 2. The cyclic voltammogram of the ionic liquid ([BMP]Tf₂N) containing 0.25 M TaF₅ and 0.25 M LiF at 200 °C on sputter-deposited Au layer. The potential was scanned from open circuit potential in negative direction and then to positive one. (a) Scan rate was 5 mV s⁻¹. (b) Scan rate was 10 mV s⁻¹. Each of two scans was done with a new working electrode.

In this study, three reduction steps were determined in a fresh ionic liquid solution, see Fig. 2 (a). The contamination of that solution was as low as possible, contrary to the voltammetry study shown in Fig. 1. Polyakova *et al.* [15] proved that three reduction peaks are related to a reduction of three

diverse tantalum species and not to reduction of one compound, such as TaF_7^{2-} complex, in three steps. By oxide titration of a molten salt system, they proved a formation of oxidized species – such as tantalum oxyfluoride $TaOF_5^{2-}$ ions and tantalum di-oxyfluorides $TaO_2F_x^{(x-1)-}$ [15], as described in the introduction. An influence of oxide impurities was expected in our study as well. As the experiments proceeded, an amount of oxide impurities and oxyfluoride ions are hypothesized to have increased gradually. The three reduction peaks observed in a first voltammetry scan disappeared in a second one, see Fig. 2 (b). The differences in the voltammetry scans might account for the presence of oxide impurities similarly to other studies [13, 14, 15]. The two voltammetry scans (Fig. 2 (b)) were recorded at the same scan rate of 10 mV s^{-1} , whereas the working electrode was renewed each time. The three reduction steps observed in the fresh ionic liquid solution (first scan) were not obtained in the contaminated solution (second and further scans). In case of contaminated solutions, there was only one step reduction observed. The three narrow cathodic peaks turned into one broad reduction peak. This elimination of the reduction steps during the cyclic voltammetry was observed many times (not showing more experiments here). Enhancing the potential limit in the negative direction (up to, e.g., -2.5 V and more) lead to faster changes of the voltammetry curves compared to experiments performed at shorter potential range (e.g., up to -1.6 V vs. Pt). Knowing the results from other studies [13, 14, 15], we might possibly conclude that the reduction of tantalum oxyfluorides eventually prevailed over the tantalum fluoride reduction. Moreover, the tantalum fluoride reduction might be possibly attributed to the first voltammetry reduction step of the three narrow steps shown in Fig. 2 (a). Verifying the first reduction step reversibility might prove that presumption. For that, electrochemical potential peak analysis is present in Supplementary.

An influence of oxide impurities upon the reduction reproducibility was observed by Polyakova *et al.* [15] at a low concentration (< 0.1 molar percent m/o) of tantalum salt K_2TaF_7 in

the molten salt FLINAK system. Therefore, increasing the TaF₅ concentration in the ionic liquid might possibly facilitate the tantalum metal electrodeposition despite some oxide impurities. (Ta electrodeposition from ionic liquid was observed by Ispas and Bund at 0.5 M TaF₅ concentration). Additionally, the tantalum reduction peaks appeared also on the anodic scan as the sweep direction was reversed, see Fig. 2. This type of behavior was observed previously for the electrodeposition of zinc from 12CE solvent [19] and from ionic liquids [20, 21]. Whitehead *et al.* [22] suggested two complementary explanations for this behavior upon zinc electrodeposition from a deep eutectic solvent. First, the electrode surface might be blocked by adsorbed solvent species which are gradually desorbed at more negative potential, secondly intermediate species needed for the reduction are formed first at more negative potentials and the electroreduction takes place more pronounced during the backward scan [20]. Another explanation for the reduction process during the reverse scan may be attributed to the formation of a potential dependent compact layer of the ionic liquid ions at the working electrode surface – observed by Atkin *et al.* – which may affect the mass transport rates of the electro active species [23].

3.2. XPS and STEM-EDX analyses of the electrodeposited coatings

The Sital glass-ceramic substrate was covered with a sputter-deposited metal layer (Nb or Au) and used for the tantalum electrodeposition. Elemental composition was investigated by STEM-EDX and X-ray photoelectron spectroscopy (XPS) on coating cross section, as well as surface, respectively. STEM was performed on two probes. A cross section of deposited specimen (from 0.4 M TaF₅ and 0.4 M LiF ionic liquid solution, cycling potential, no post-treatment, no stirring) was performed using gallium ion etching with top protective carbon cap, as shown in Fig. 3. Cavities were observed between Au deposited substrate and Ta-based deposit causing a very low adhesion of the coating. A post-depositional washing was excluded in that case as the coating

might detach completely. This specimen was not annealed either. The ionic liquid became dry on the surface forming about 150 nm “oxyfluorides” thick layer with small Ta content. The Ta-based coating was found underneath having thickness of about 1,430 nm. Additionally, ca. 150 nm thick oxide (with silicon and aluminum content) bottom layer was detected between Au deposited substrate and Ta coating. Both oxides and fluorides were accumulated mainly on the top and bottom of the Ta coating, see Fig. 4. Inside the deposited coating, O (37 at. %) was distributed homogenously, whereas F (15 at. %) content increased with the coating thickness by about 5 at.%. Additionally, Si (20 at. % / 15 wt. %) was analyzed as well. All these elements were part of the Ta (11 at. % / 53 wt. %) coating, see Table 1 for the atomic and weight elemental fractions and Fig. 5 for element distribution across the Ta coating. Impurities (O, Si, Al) in Ta were caused by fluoride reaction with glass-ceramic working electrode. The bottom impurity oxide layer (O, Si, Al) was formed during a pre-heating step, taking about 43 s before the electrodeposition start. Stirring rate at that specimen was set to zero. Due to high fluoride concentration (2 x 0.4 M) and high working temperature of 200 °C, the Sitall substrate etching rate was enhanced compared to lower fluoride concentration and lower temperature in the second specimen investigated by the STEM analysis, see below. The thick coating (1,430 nm) shown here also obtains large amount of carbon (11 at. %) and fluorides (15 at. %) if compared to the second thin specimen tested by STEM. Considering the element distribution plot, as well as the color EDX maps in Fig. 4, the coating composition appears quite uniform and shows that the deposition was not too affected by changes in local ionic concentrations.

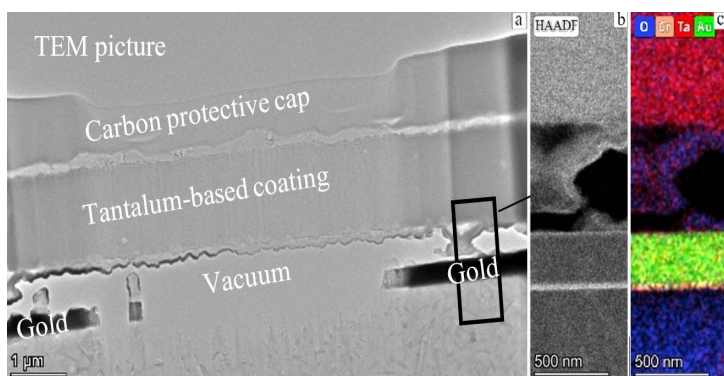


Fig. 3. Focused ion beam (FIB) cross section of tantalum-based coating on gold / Sitall glass-ceramic substrate (a) TEM overview image, (b) HAADF - STEM (high-angle annular dark field scanning transmission) picture and (c) EDX color mix map (O-K, Cr-K, Ta-L, Au-L) origin from same sample cross section. (*Deposited by cycling from -1.4 V to -1.7 V and back to -1.4 V vs. Pt, at zero stirring rate from 0.4 M TaF₅ and 0.4 M LiF in [BMP]Tf₂N ionic liquid solution*).

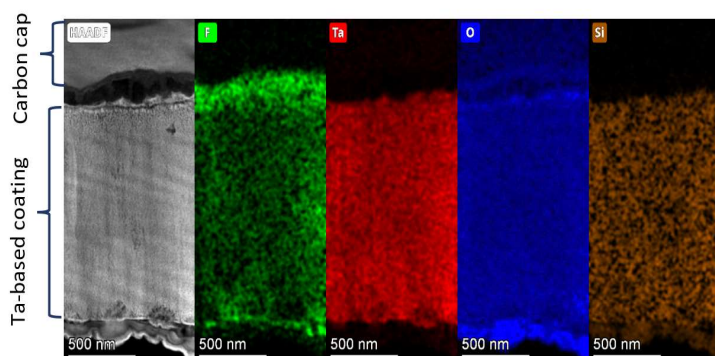


Fig. 4. HAADF - STEM image and corresponding STEM-EDX elemental mapping of tantalum-based coating FIB cross section upon gold / Sitall glass-ceramic substrate. Same specimen as in Fig. 3. (*Deposited by cycling from -1.4 V to -1.7 V and back to -1.4 V vs. Pt, at zero stirring rate from 0.4 M TaF₅ and 0.4 M LiF in [BMP]Tf₂N ionic liquid solution*).

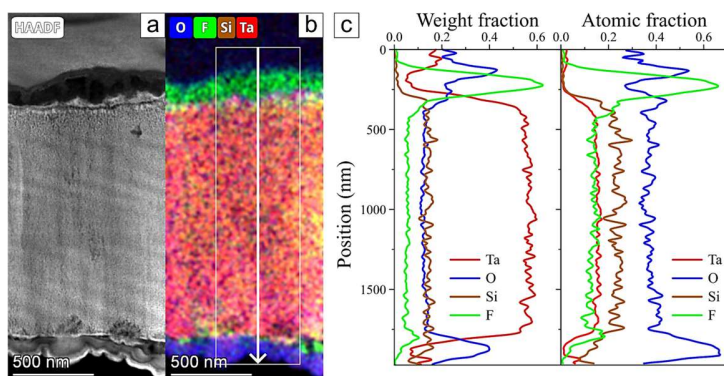


Fig. 5. FIB cross section of tantalum-based coating on gold / Sitall glass-ceramic substrate (a) HAADF - STEM picture, (b) corresponding EDX color mix map (O-K, F-K, Si-K, Ta-L), (c) spectrum profile plot showing element distribution as weight and atomic fraction across tantalum-based coating. Same specimen as in Fig. 4. (Electrodeposited by cycling from -1.4 V to -1.7 V and back to -1.4 V vs. Pt, at zero stirring rate from 0.4 M TaF_5 and 0.4 M LiF in $[\text{BMP}]\text{Tf}_2\text{N}$ ionic liquid solution).

Table 1 Compositional fractions inside the tantalum-based coating, of which cross section was shown in Fig. 4 and Fig. 5.

Element	Family	Atomic Fraction (%)	Atomic Error (%)	Mass Fraction (%)	Mass Error (%)	Fit Error (%)
C	K	10.59	1.92	3.37	0.62	17.43
O	K	37.34	5.15	15.83	2.89	2.56
F	K	15.26	2.95	7.68	1.54	3.33
Al	K	4.8	1.02	3.43	0.71	3.49
Si	K	20.38	3.56	15.17	2.68	0.75
Ca	K	0.26	0.04	0.28	0.04	1.65
Ti	K	0.1	0.02	0.12	0.02	0.76
Ta	L	11.1	1.48	53.22	3.66	0.27
Au	L	0.17	0.02	0.9	0.11	1.75

Moreover, potentiostatic deposition was performed at a constant stirring rate. Three coating trials were performed from the same ionic liquid solution (0.25 M TaF_5 and 0.25 M LiF) successively and analyzed by the XPS technique. High resolution spectra of Ta 4f and F 1s are shown in Fig. 6 (a-c). The upper row in the figure shows the Ta 4f peaks (together with F 2s), whereas the lower one the F 1s spectra. F/Ta atomic ratios were evaluated using broad XPS survey spectra (not

shown) for all the studied specimens. The very high atomic % F/Ta ratio up to 88 in the second trial was most probably due to excluded surface washing in that case. The F/Ta ratio in the first and third trial was 10 and 5 at. %, respectively. According to the high-resolution spectra, the fluorides were present in a form of LiF, C-F bonds and even Ta-F and Al-F in the last deposition trial. LiF peak position in F 1s spectra differed in the first (684.5 eV) and second (685.9 eV) deposition trial case, however, in Li 1s spectra (not shown) their positions were similar, 56.2 eV and 56.5 eV, respectively. We could not explain that peak position shift, but it might be, e.g., due to a gradual formation of oxyfluorides during each deposition step trial. Li⁺ ions in the solution facilitate tantalum electrodeposition in a way that they disrupt the Ta-F bonds as the fluorides bind preferentially to lithium [9]. Presence of TaF₅ in the last deposition trial induces a large rise in fluoride ions at the growing edge of the deposit. The excess of F⁻ ions might require further cations to maintain local charge electroneutrality. AlF₃ compound found in the third deposit surface accounts for presence of cations dissolved from the ceramic substrate by fluorides present in the ionic solution. The specimen with the highest F/Ta ratio was annealed at 800 °C for 6 h (pressure ranging from 10⁻³ to 10⁻⁴ Pa) and analyzed again, see Fig. 7. Lithium was eliminated together with fluorides. Carbon-fluoride bonds disappeared as well, whereas TaC_x (x ~ 1.6) raised newly after the annealing. The annealed specimen was consequently tested by STEM analysis. Alternatively, to the first STEM analysis shown above, the second specimen was deposited at constant potential of -1.7 V vs. Pt and constant magnetic stirring rate.

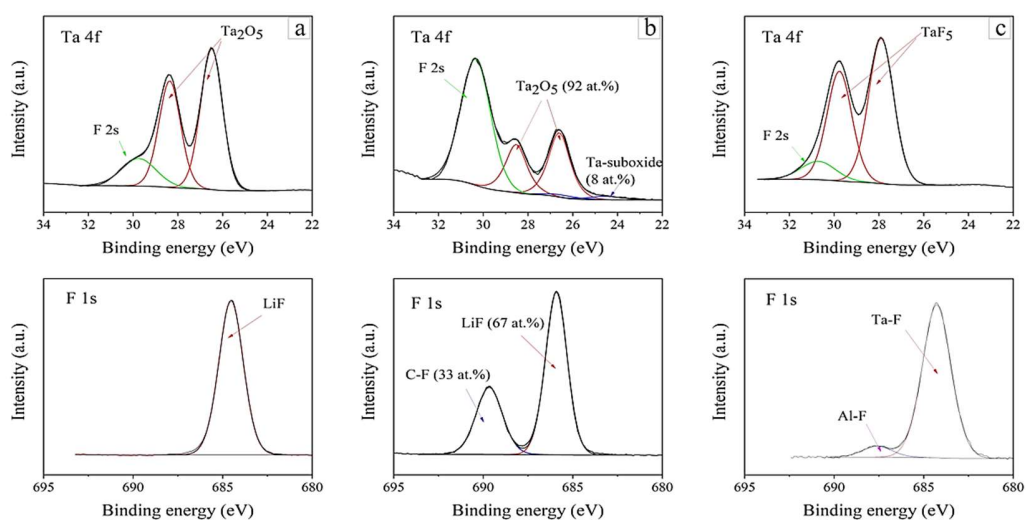


Fig. 6. XPS analyses of Ta-based coatings (a) first deposition trial on Nb substrate, deposited at -1.5 V vs. Pt (at 500 rpm), 90 nm thick, (b) second trial on Nb, -1.7 V (900 rpm), 240 nm thick, (c) third trial on Au substrate, -1.5 V, ca 100 nm thick.

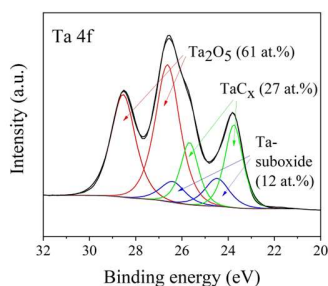


Fig. 7. XPS of second trial specimen (on Nb, thickness 240 nm) after annealing at 800 °C for 6 h (10^{-3} to 10^{-4} Pa).

The STEM analysis of Ta-based coating cross section (240 nm) on Nb deposited Sital glass ceramic substrate is shown in Fig. 8. F-free surface was obtained after the annealing treatment at 800 °C for 6 h (10^{-3} to 10^{-4} Pa). Similarly, to the first STEM analysis, there is a thin fluorine containing strip just underneath the Ta-based coating. A reason why a F-strip gets formed before the Ta coating starts to grow is unknown. Li could not be analyzed by that device. Therefore, we could not clearly analyze a type of the fluorine compound. Elemental analyses within the Ta-

coating revealed F content less than 4 at. %, O - 40 at. %, Si - 27 at. % (14 wt. %) and Ta - 21 at. % (70 wt. %). The elemental distribution is shown in Fig. 9 and the weight and atomic fractions averaged from the inside of the Ta-based layer are given in Table 2. The 4 at. % F content obtained is a good result together with the low carbon content (3 at. %). The annealing was probably the main reason of the significant F and C decrease if compared to the first STEM analysis made on sample without annealing. The annealing effect was proved also by the XPS analysis, discussed already above. The Si atomic content was still high (comparable to the first STEM specimen analysis). Moreover, we observed clear changes in the O content distribution across the Ta coating. The initial, 50 nm thick, Ta-based coating contained the highest Ta/O ratio, see position 220-250 nm in the EDX spectrum profile, shown in Fig. 9. The O content was about 32 at. % in the very initial thin coating, whereas on the surface it reached about 40 at. %.

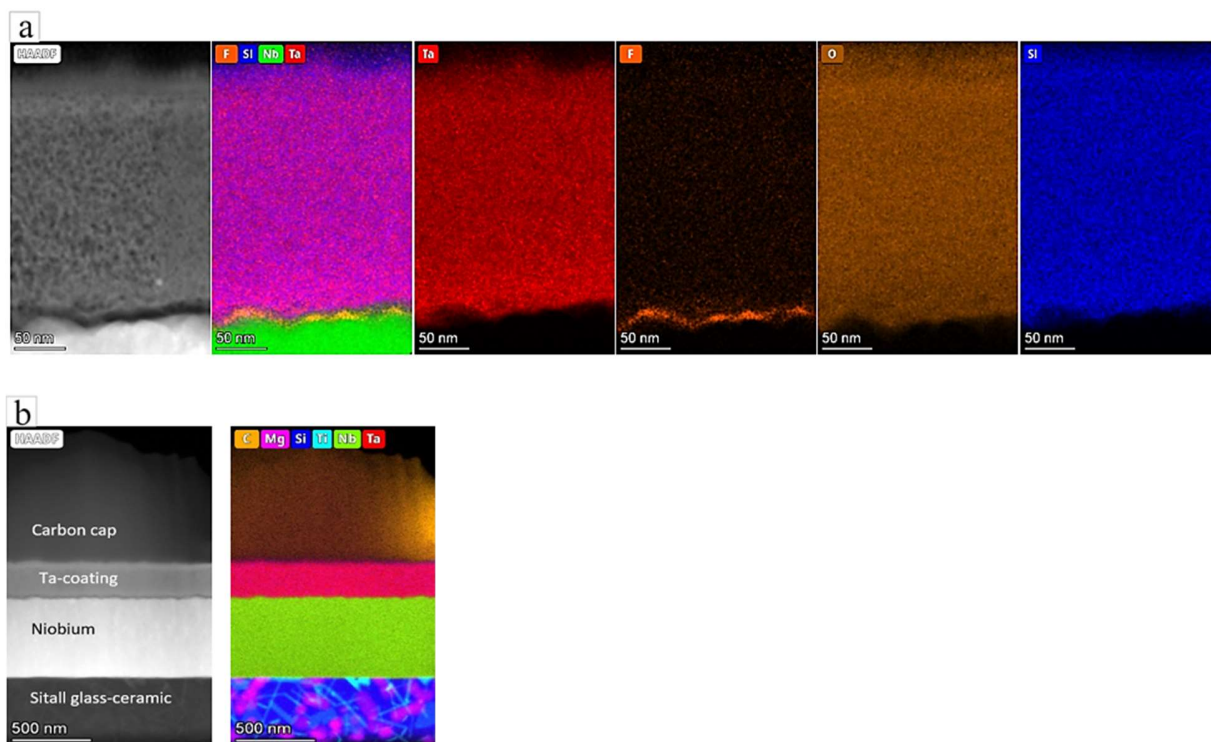


Fig. 8. HAADF - STEM image and corresponding STEM-EDX elemental mapping of Ta-based coating FIB cross section on Nb / Sitall glass-ceramic substrate at (a) higher and (b) lower magnification. (*Electrodeposited at constant*

potential -1.7 V vs. Pt, at constant stirring rate of 900 rpm from 0.25 M TaF_5 and 0.25 M LiF in $[\text{BMP}]\text{Tf}_2\text{N}$ ionic liquid solution). Annealed at 800 °C.

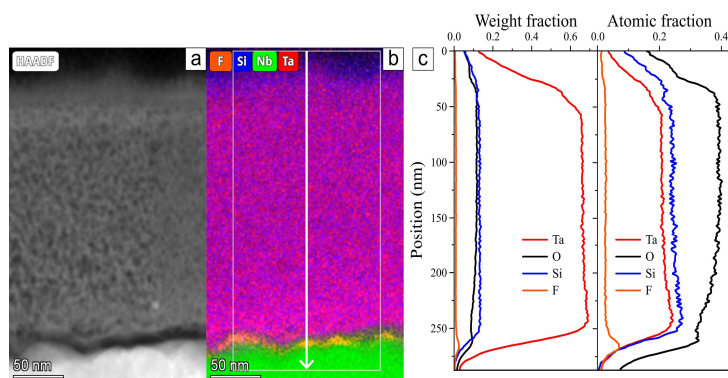


Fig. 9. FIB cross section of tantalum-based coating on Nb / Sitall glass-ceramic substrate (a) HAADF - STEM picture, (b) corresponding EDX color mix map (F-K, Si-K, Nb-K, Ta-L), (c) spectrum profile plot showing element distribution as weight and atomic fraction across tantalum-based coating. Same specimen as in Fig. 8. (Electrodeposited at constant potential -1.7 V vs. Pt, at constant stirring rate of 900 rpm from 0.25 M TaF_5 and 0.25 M LiF in $[\text{BMP}]\text{Tf}_2\text{N}$ ionic liquid solution). Annealed at 800 °C.

Table 2 Compositional fractions inside the tantalum-based coating, of which cross section was shown in Fig. 8 and Fig. 9.

Element	Family	Atomic Fraction (%)	Atomic Error (%)	Mass Fraction (%)	Mass Error (%)	Fit Error (%)
C	K	4.1	0.41	0.9	0.08	2.7
N	K	1.9	0.42	0.5	0.11	4.66
O	K	40.0	5.31	12.0	2.32	0.75
F	K	3.8	0.83	1.3	0.29	4.81
Na	K	2.9	0.63	1.2	0.27	2.64
Si	K	26.8	4.39	14.2	2.59	1.28
Se	K	0.3	0.04	0.4	0.06	0.49
Ta	L	20.4	2.63	69.5	3.41	0.11

3.3. Structural properties. XRD

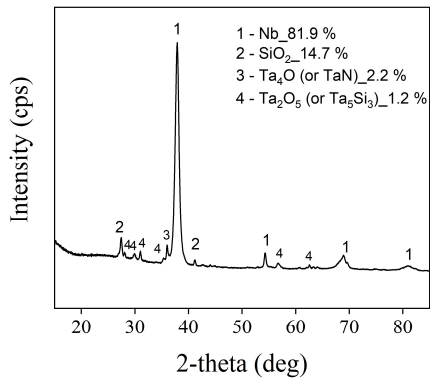


Fig. 10. X-ray analysis of annealed Ta-based coating electrodeposited on Nb coated Sitall substrate from 0.25 M TaF₅ and 0.25 M LiF solution at 150 °C (same as the second STEM specimen), annealed at 800 °C for 6 h (10⁻³ to 10⁻⁴ Pa).

X-ray diffraction (XRD) analysis plot of Ta-based coating after annealing is shown in Fig. 10. Crystalline Ta was not proved as the largest peaks in the plot were most probably niobium. Ta (bcc) and Nb (bcc) are not distinguishable by the XRD analysis. Both Nb and Au overlap with Ta, therefore these metals are insufficient as underlayers for Ta detection using diffractometry analysis. For future experiments platinum substrate might be a better choice. Si was detected as SiO₂ (P3221_156196 ICSD), Ta₂O₅ (Ibam_250052 ICSD) and Ta₄O (Pmmm_03-065-6450 ICDD, or TaN) were determined by XRD as well. Ta₂O₅ was proved before by X-ray photoelectron spectroscopy (XPS). For better selectivity Nb, Au and tungsten shall be excluded as underlayers in Ta deposition processes.

4. Conclusions

Electrodeposition of tantalum thin coating was attempted from a room temperature ionic liquid BMP[Tf₂N] in presence of dissolved TaF₅ and LiF. Wrong choice of working electrode material (gold or niobium deposited on glass-ceramic) lead to a serious deterioration of Ta purity. Fluoride-

containing ionic liquid solution in contact with glass material accounted for the experimental failure. Glass, quartz, and mica substrates covered with Au were commonly applied in previous studies too. However, no detailed analyses on silicon content inside the Ta coating electrodeposited from an ionic liquid were performed. Our study presented detailed analyses of the electrodeposited Ta. Elemental distribution in two Ta-coatings along their cross sections was obtained. Moreover, influence of annealing was tested, whereas reduction of F on the surface (XPS analysis), as well as inside (STEM-EDX) of the coating was substantial. The high F/Ta ratio (88 at. %) on the surface turned to zero after the annealing. Lithium was also fully eliminated from the surface (XPS). F content inside the Ta-coating (STEM-EDX) was about 15 at. % in the first tested specimen (not annealed) and about 4 at. % in the second specimen (annealed one). Carbon content was about 11 at. %, and 4 at. %, respectively. In the annealed specimen, there were three main elements – Ta, Si and O. Ta reached average concentration of about 20 at. % (70 wt. %), Si about 27 at. % (14 wt. %), and O 40 at. % (12 wt. %) inside of the annealed specimen. The O content was about 32 at. % in the very initial thin coating, and the initial O/Ta atomic ratio was about 1.3 (annealed case). Using the same ionic liquid solution for a prolonged time, F bonds with tantalum Ta-F and aluminum Al-F in the coating were determined too (XPS). Al traces detected as AlF₃ compound originated from the ceramic substrate, as well as Si and O. The cyclic voltammetry changes (three narrow cathodic peaks turned into one broad reduction peak) accounted for compositional variations due to ceramic-based substrate dissolution. Irreversible electroreduction was analogous to a molten salt system deposition in presence of oxide impurities. Ta₂O₅ was determined by both XPS, as well as XRD analyses. High amount of crystalline SiO₂ was proved by the XRD analysis. Crystalline Ta could not be clearly verified due to unluckily chosen metal underlayer material. Both, Au and Nb overlap with Ta in the XRD spectra. In future, detailed understanding of Ta electrodeposition might help to reach better purity Ta coatings.

Acknowledgement

The work was done under the Czech Grant Agency project no. 22-14886S. CzechNanoLab project LM2023051 funded by MEYS CR is gratefully acknowledged for the financial support of the sample fabrication at CEITEC Nano Research Infrastructure.

References

- [1] M. Nahra, L. Svecova, N. Sergent, and E. Chaînet, Thin tantalum film electrodeposition from an ionic liquid - Influence of substrate nature, electrolyte temperature and electrochemical parameters on deposits quality, *J. Electrochem. Soc.* 168 (2021) 082501. <https://doi.org/10.1149/1945-7111/ac1697>.
- [2] G. Eranna, B. C. Joshi, D. P. Runthala, and R. P. Gupta, Oxide materials for development of integrated gas sensors - A comprehensive review, *Crit. Rev. Solid State Mater. Sci.* 29 (2004) 111-188. <https://doi.org/10.1080/10408430490888977>.
- [3] S. Kim, Hydrogen gas sensors using a thin Ta₂O₅ dielectric film, *J. Korean Phys. Soc.* 65 (2014) 1749-1753. <https://10.3938/jkps.65.1749>.
- [4] B.-Y. Liu, W.-C. Liu, New room temperature ammonia gas sensor synthesized by a tantalum pentoxide (Ta₂O₅) dielectric and catalytic platinum (Pt) metals, *IEEE Trans. Electron Devices* 67 (2020) 2566-2572.
- [5] P. Schütte, U. Näher, Tantalum supply from artisanal and small-scale mining: A mineral economic evaluation of coltan production and trade dynamics in Africa's Great Lakes region, *Resour. Policy* (2020) 101896.
- [6] N.A. Mancheri, B. Sprecher, S. Deetman, S.B. Young, R. Bleischwitz, L. Dong, R. Kleijn, A. Tukker, Resilience in the tantalum supply chain, *Resour. Conserv. Recycl.* 129 (2018) 56-69.
- [7] L. Xia, X. Wei, H. Wang, F. Ye, Z. Liu, Valuable metal recovery from waste tantalum capacitors via cryogenic crushing-alkaline calcination-leaching process, *J. Mater. Res. Technol.* 16 (2022) 1637-1646. <https://doi.org/10.1016/j.jmrt.2021.12.104>.
- [8] A.P. Abbott, K.J. McKenzie, Application of ionic liquids to the electrodeposition of metals, *Phys. Chem. Chem. Phys.* 8 (2006) 4265-4279. <http://dx.doi.org/10.1039/B607329H>.
- [9] F. Endres, A.P. Abbot, D.R. MacFarlane, *Electrodeposition from Ionic Liquids*, Wiley-VCH, Weinheim, Germany, pp. 114-116, 2008.
- [10] S.Z. El Abedin, H.K. Farag, E.M. Moustafa, U. Welz-Biermann, F. Endres, Electroreduction of tantalum fluoride in a room temperature ionic liquid at variable temperatures, *Phys. Chem. Chem. Phys.* 7 (2005) 2333-2339. <https://doi.org/10.1039/b502789f>.
- [11] M. Nahra, L. Svecova, E. Chaînet, Pentavalent tantalum reduction mechanism from 1-butyl-3-methyl pyrrolidinium bis(trifluoromethylsulfonyl)imide ionic liquid, *Electrochim. Acta* 182 (2015) 891-899. <https://doi.org/10.1016/j.electacta.2015.09.106>.
- [12] N. Borisenko, A. Ispas, E. Zschippang, Q.X. Liu, S.Z.E. Abedin, A. Bund, F. Endres, In situ STM and EQCM studies of tantalum electrodeposition from TaF₅ in the air- and water-stable ionic liquid 1-butyl-1-methylpyrrolidinium bis(trifluoromethylsulfonyl)amide, *Electrochim. Acta* 54 (2009) 1519-1528. <https://doi.org/10.1016/j.electacta.2008.09.042>.
- [13] F. Lantelme, A. Barhoun, G. Li, J.P. Besse, Electrodeposition of Tantalum in NaCl - KCl - K₂TaF₇ Melts, *J. Electrochem. Soc.* 139 (1992) 1249. <https://doi.org/10.1149/1.2069392>.
- [14] P. Chamelot, P. Taxil, B. Lafage, Voltammetric studies of tantalum electrodeposition baths, *Electrochim. Acta* 39 (1994) 2571-2575. [10.1016/0013-4686\(94\)00262-2](https://doi.org/10.1016/0013-4686(94)00262-2).

-
- [15] L.P. Polyakova, E.G. Polyakov, F. Matthiesen, E. Christensen, N.J. Bjerrum, Electrochemical study of tantalum in fluoride and oxofluoride melts, *J. Electrochem. Soc.* 141 (1994) 2982. <https://doi.org/10.1149/1.2059269>.
- [16] P. Chamelot, P. Palau, L. Massot, A. Savall, P. Taxil, Electrodeposition processes of tantalum(V) species in molten fluorides containing oxide ions, *Electrochim. Acta* 47 (2002) 3423-3429. [https://doi.org/10.1016/S0013-4686\(02\)00278-5](https://doi.org/10.1016/S0013-4686(02)00278-5).
- [17] A. Ispas, B. Adolphi, A. Bund, F. Endres, On the electrodeposition of tantalum from three different ionic liquids with the bis(trifluoromethyl sulfonyl) amide anion, *Phys. Chem. Chem. Phys.* 12 (2010) 1793-1803. <https://doi.org/10.1039/B922071M>.
- [18] A. Ispas, A. Bund, F. Endres, Application of the electrochemical quartz crystal microbalance for the investigation of metal depositions from ionic liquids, *ECS Trans.* 16 (2009) 411-420.
- [19] L. Vieira, A.H. Whitehead, B. Gollas, Mechanistic studies of zinc electrodeposition from deep eutectic electrolytes, *J. Electrochem. Soc.* 161 (2014) D7. <https://doi.org/10.1149/2.016401jes>.
- [20] T.J. Simons, A.A.J. Torriero, P.C. Howlett, D.R. Macfarlane, M. Forsyth, High current density, efficient cycling of Zn²⁺ in 1-ethyl-3-methylimidazolium dicyanamide ionic liquid: The effect of Zn²⁺ salt and water concentration, *Electrochem. Commun.* 18 (2012) 119-122. [10.1016/J.ELECOM.2012.02.034](https://doi.org/10.1016/J.ELECOM.2012.02.034).
- [21] T.J. Simons, P.C. Howlett, A.A.J. Torriero, D.R. Macfarlane, M. Forsyth, Electrochemical, transport, and spectroscopic properties of 1-ethyl-3-methylimidazolium ionic liquid electrolytes containing zinc dicyanamide, *J. Phys. Chem. C* 117 (2013) 2662-2669. DOI:10.1021/JP311886H.
- [22] A.H. Whitehead, M. Pölzler, B. Gollas, Zinc electrodeposition from a deep eutectic system containing choline chloride and ethylene glycol, *J. Electrochem. Soc.* 157 (2010). DOI:10.1149/1.3364930.
- [23] R. Atkin, N. Borisenko, M. Druschler, S.Z. El Abedin, F. Endres, R. Hayes, B. Huber, B. Roling, An in situ STM/AFM and impedance spectroscopy study of the extremely pure 1-butyl-1-methylpyrrolidinium tris(pentafluoroethyl)trifluorophosphate/Au(111) interface: potential dependent solvation layers and the herringbone reconstruction, *Phys. Chem. Chem. Phys.*, 13 (2011) 6849-6857. <https://doi.org/10.1039/C0CP02846K>.